JOURNAL OF SOLID STATE CHEMISTRY 42, 251–262 (1982)

The Structures of Lithium-Inserted Metal Oxides: $LiReO_3$ and Li_2ReO_3

R. J. CAVA,* A. SANTORO,† D. W. MURPHY,* S. ZAHURAK,*AND R. S. ROTH†

*Bell Laboratories, Murray Hill, New Jersey 07974, and †National Bureau of Standards, Washington, D.C. 20234

Received October 13, 1981; in revised form December 28, 1981

The crystal structures of $LiReO_3$ and Li_2ReO_3, obtained by Li insertion into ReO_3, were determined by neutron diffraction powder profile analysis. For both phases, the ReO_3 host lattice, made exclusively of corner-shared octahedra, was altered significantly on Li insertion without breaking bonds. The original 12-coordinated perovskite-like cavity was changed into two octahedral sites, which are occupied by the lithium ions.

There has been significant interest in recent years in materials which undergo topotactic insertion of lithium because of their potential use as electrode materials in secondary batteries (*1–3*). Lithium is ionic in these compounds, and the charge is compensated by a reduction of the host cations (chalcogen–chalcogen bonds may be reduced in some compounds). Host structures may be of the layer or framework type. In the layer type, the Li^+ ions are accommodated in the van der Waals gap between layers, and in framework structures, Li^+ ions occupy formerly vacant cations sites. ReO_3 and shear structures related to it are suitable hosts for lithium (*3–5*), with Li_xReO_3 forming three distinct phases with stoichiometries (*5*) $0.0 \leq x \leq 0.35$, $x = 1.0$, and $1.8 \leq x \leq 2.0$. Structural characterization of insertion compounds has lagged far behind the preparation of new compounds due to the unavailability of single crystals for standard crystallographic structure analysis. Lithium insertion inevitably involves significant changes in structural dimensions which pulverize starting materials. Neutron diffraction powder profile analysis is the best technique for structure determination, as it requires only a polycrystalline powdered sample, and is more sensitive than X-ray diffraction in the characterization of light atoms such as Li in structures which contain atoms of higher atomic number. The method has been applied to lithium insertion compounds of TiS_2 (*6*), WO_3 (*7*), and MoO_2 (*8*). We report here in detail on the structures of $LiReO_3$ and Li_2ReO_3, elaborating on an earlier communication (*9*). The low-lithium compound $Li_{0.35}ReO_3$ could not be prepared in large batches in single-phase form and its structure was therefore not determined.

Experimental

ReO_3 is red in color and displays metallic conductivity. The ReO_3 employed in this study (Alfa Inorganics) was purified by iodine transport in a 450–400°C gradient. Finely intergrown with the resulting ReO_3 crystals was about 5% of a second phase which powder X-ray diffraction showed to

0022-4596/82/060251-12$02.00/0

be ReO_2. Although this phase was present throughout the insertion reactions and structural characterization, its effect on the structural analysis was easily eliminated by omitting a few small regions of the neutron diffraction powder pattern where diffracted intensities interfered with those of the major phase.

Details of the phase equilibria for Li_xReO_3 have been reported elsewhere (*5*). The Li_2ReO_3 used in the structural study was prepared by adding a solution of *n*-butyl–lithium in hexane (54 ml, 2.46 *N*) to powdered ReO_3 (22.82 g) in a Pyrex vessel. After an initial exothermic reaction, the vessel was sealed under reduced pressure and heated to 50°C for 7 days. The reaction mixture was opened in a helium atmosphere glovebox, filtered, washed with hexane, and dried *in vacuo*. A small sample treated with a standard iodine solution in acetonitrile determined the lithium stoichiometry to be $Li_{1.95}ReO_3$.

It did not prove practical to prepare homogeneous $LiReO_3$ directly from ReO_3. Rather, it was prepared by treating solid Li_2ReO_3 with absolute ethanol under argon in a Schlenk frit. In that process, hydrogen gas is evolved and soluble lithium ethoxide is formed. Over 2 days the solid was filtered and more ethanol was added. The filtrates were titrated for base to monitor the lithium removed. When the stoichiometry was close to $LiReO_3$, the X-ray powder patterns were monitored until a pure phase was formed. Excessive washing with ethanol must be avoided near the end of the reaction, as the cubic $Li_{0.35}ReO_3$ phase slowly appears as more lithium is removed. After single-phase $LiReO_3$ was formed, the sample was dried *in vacuo*.

Neutron diffraction measurements were performed on a powder diffractometer at the NBS Reactor, with the experimental conditions described in Table I. The samples were loaded into 1-cm-diameter vanadium cans sealed with wax to avoid decomposition of the compounds, which are air sensitive.

The powder profile refinement was performed with the Rietveld method (*10*) adapted to the five-detector diffractometer design and modified to allow the refinement of background intensity (*11*). In the course of this analysis, it became apparent that the peaks produced by samples of the two compounds did not conform to a Gaussian distribution. This effect cannot be attributed to instrumental factors, since the diffractometer, used with identical conditions and with standard materials such as Al_2O_3, gives Gaussian diffraction lines over the entire 2Θ angular range within very good approximation (χ between 1.1 and 1.2, by fitting single peaks). The program was then further modified to describe the line profiles with the Pearson Type VII distribution, which allows the lineshape to be changed continuously from Gaussian to Lorentzian through one additional profile parameter. The main properties of the function and its application and interpretation to the present problem are described in detail elsewhere (*12*).

The neutron-scattering amplitudes em-

TABLE I

EXPERIMENTAL CONDITIONS USED TO MEASURE THE POWDER PATTERNS OF $LiReO_3$ AND Li_2ReO_3

Monochromatic beam:	reflection 220 of a Cu monochromator with mosaic spread of ~15′ arc
Wavelength:	1.542(1) Å
Filter:	pyrolitic graphite
Horizontal divergences:	10, 20, and 10′ arc for the inpile, monochromatic beam, and diffracted beam collimators, respectively
Sample container:	vanadium can of ~10-mm diameter
Angular ranges scanned by each of the five detectors:	15–40, 35–60, 55–80, 75–100, 95–120°; step: 0.05°

ployed were $b(\mathrm{Li}) = -0.214$, $b(\mathrm{Re}) = 0.92$, and $b(\mathrm{O}) = 0.58$ ($\times 10^{-12}$ cm) (*13*). Initial lattice parameters were obtained by least-squares fits to the X-ray diffraction data. The background was assumed to be a straight line with finite slope and was refined for each channel. This description is, in general, adequate within the small angular interval scanned by each counter. Approximate values of the background parameters were obtained at positions in the patterns free from diffraction effects. In the refinement of the structural models, all structural, lattice, and profile parameters were refined simultaneously. Refinements were terminated when all parameter shifts were less than 0.3σ.

Results

Precise rhombohedral unit cell dimensions for both $LiReO_3$ and Li_2ReO_3 were obtained by least-squares fits of the peak positions in powder X-ray diffraction patterns, indicating that an earlier preliminary orthorhombic indexing (*4*) was inaccurate. The X-ray powder diffraction patterns and unit cell parameters for $Li_{0.35}ReO_3$, $LiReO_3$, and Li_2ReO_3 are presented in Table II. We did not observe a doubling of the cubic ReO_3-type cell for $Li_{0.35}ReO_3$ in the X-ray powder patterns, as is observed in the analogous compound $Li_{0.36}WO_3$ (*7*). After indexing and unit cell parameters were established, it was apparent that the structures of $LiReO_3$ and Li_2ReO_3 were closely related to those of many of the transition metal trifluorides and ferroelectric $LiNbO_3$. The initial atomic positions for all atoms of $LiReO_3$ and for the rhenium, oxygen, and half of the lithium atoms of Li_2ReO_3 were

TABLE II

CRYSTALLOGRAPHIC DATA

	ReO_3	$Li_{0.35}ReO_3$	$LiReO_3$	Li_2ReO_3
z	1	1	6	6
a_0	3.748	3.690	5.0918(3)	4.9711(1)
c_0	—	—	13.403(1)	14.788(1)
Vol/FU	52.65	50.24	50.16	52.74

X-Ray powder patterns

$Li_{0.35}ReO_3$			$LiReO_3$			Li_2ReO_3	
HKL	*d*	I/I_0	*HKL*	*d*	I/I_0	*d*	I/I_0
100	3.690	100	012	3.684	100	3.720	100
110	2.609	95	104	2.668	65	2.805	60
111	2.130	40	110	2.546	50	2.486	50
200	1.845	45	006	2.234	5	—	—
210	1.650	80	113	2.212	5	2.219	5
211	1.506	45	202	2.094	30	2.067	30
220	1.305	20	024	1.842	35	1.860	35
300	1.230	40	116	1.679	30	1.750	55
			122	1.617	25	1.589	30
			018	1.566	10	1.699	20
			214	1.492	20	1.489	20
			300	1.470	10	1.435	15
			208	—	—	1.402	15
			1010	—	—	1.399	

TABLE III

A. The structure of $LiReO_3$

Atom	Position	X	Y	Z	B (Å^2)
Re	6*a*	0	0	0	0.18(6)
Li	6*a*	0	0	0.273(1)	1.6(3)
O	18*b*	−0.3801(7)	0.012(1)	0.2460(9)	0.27(6)

m = 1.5 (*12*), R_N = 5.66, R_p = 5.55, R_w = 7.04, R_E = 5.00. Space group: $R3c$, Z = 6. Number of observations: 2464. Number of independent Bragg reflections: 49.

B. The structure of Li_2ReO_3

Atom	Position	X	Y	Z	B^a (Å^2)
Re	6*a*	0	0	0	0.21(6)
Li1	6*a*	0	0	0.312(1)	1.4(3)
Li2	6*a*	0	0	0.169(1)	1.4(3)
O	18*b*	−0.3580(9)	−0.008(2)	0.2551(8)	0.21(6)

m = 3 (*12*), R_N = 8.05, R_p = 7.58, R_w = 9.77, R_E = 7.71. Space group: $R3c$, Z = 6. Number of observations: 2505. Number of independent Bragg reflections: 65.

[a] Thermal parameters not refined independently for this coupound:

$$R_N = \frac{\Sigma|I(\text{obs}) - I(\text{calc})|}{\Sigma I(\text{obs})},$$

$$R_p = \frac{\Sigma|y(\text{obs}) - y(\text{calc})|}{\Sigma y(\text{obs})},$$

$$R_w = \left|\frac{\Sigma w[y(\text{obs}) - y(\text{calc})]^2}{\Sigma w[y(\text{obs})]^2}\right|^{1/2},$$

$$R_E = \left|\frac{N - P + C}{\Sigma w[y(\text{obs})]^2}\right|^{1/2},$$

where N = number of independent observations, p = number of parameters, C = number of constraints, y = counts at angle 2Θ, I = integrated Bragg intensities, and w = weights. The present atomic coordinates are related to those in Ref. (12), Table I, by inversion and translation of the cell origin by 0.5c.

therefore taken as those of $LiNbO_3$ (*14*), transformed to a coordinate system in which they would be compatible with the positions reported in the transition metal trifluorides. The extra lithium atoms present in the structure of Li_2ReO_3 were assigned on the basis of chemical considerations. Rhombohedral structures of the MF_3 and $LiNbO_3$ types have been described in the space groups $R\bar{3}c$ and $R3c$. For both $LiReO_3$ and Li_2ReO_3 the structures are noncentrosymmetric, space group $R3c$. Dropping the space group symmetry to $R3$ through elimination of the c glide did not,

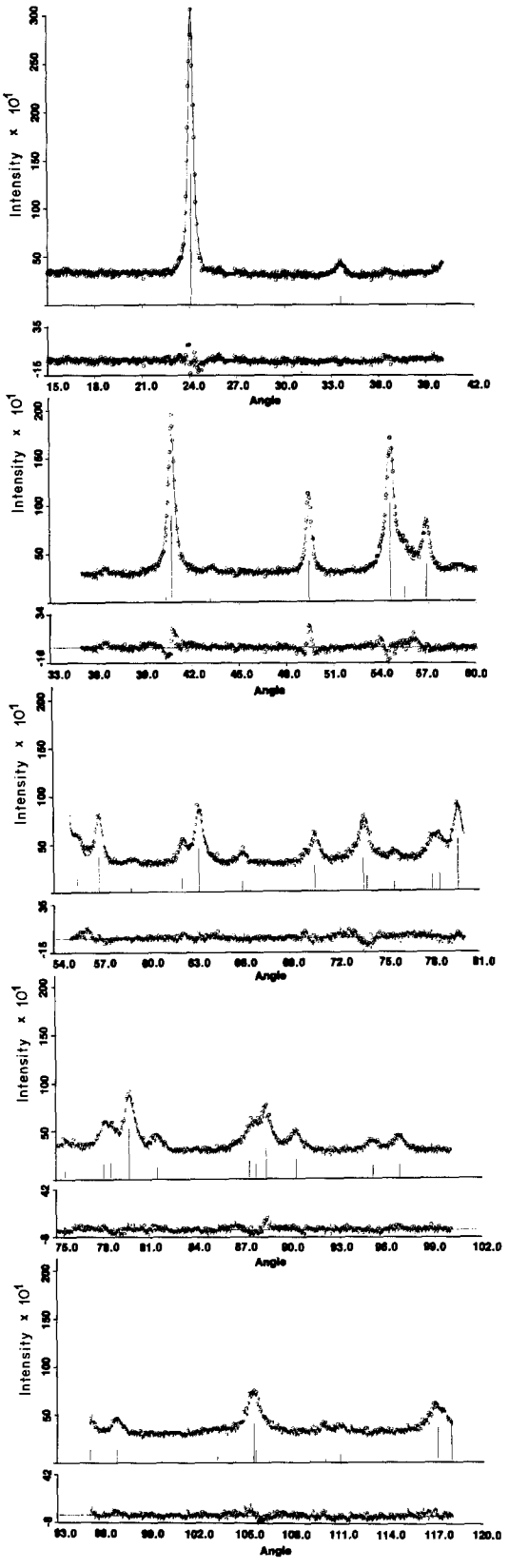

in either case, improve the refinement agreement factors or result in significant shifts of the atoms from their $R3c$ positions.

$LiReO_3$

The refinement in $R3c$ led to excellent agreement between the final model and the data (see Table III and Fig. 1). The diffracted lineshapes were found to be nearly Lorentzian. There are six formula units per hexagonal cell. Both Li and Re were found to occupy positions of the type $6a$, while the oxygen atoms are in the general position $18b$. Atomic positions and thermal parameters for the $LiReO_3$ structure are presented in Table III A.

The structure consists of chains of occupied or vacant face-shared MO_6 octahedra, running parallel to the hexagonal c axis. Neighboring chains of face-shared octahedra share only edges. There are three chains per cell, with six octahedra in each chain defining c. A projection of the structure down c is presented in Fig. 3. The MO_6 octahedra are irregular, as can be seen in the figure, which emphasizes the shared triangular faces for two of the chains. Beginning with the Re at (0, 0, 0), the MO_6 octahedra are occupied in the sequence Re–Li–vacancy–Re–Li–vacancy. The refinements indicate that the Li atoms are ordered, and do not occur in significant concentrations in the "vacant" oxygen octahedra. The structure is diagrammed perpendicular to the chains in Fig. 5, where a comparison of the structures of ReO_3, $LiReO_3$, and Li_2ReO_3 is made.

Li_2ReO_3

As for $LiReO_3$, the refinement in $R3c$ led to excellent agreement between the final

FIG. 1. Observed and calculated powder neutron diffraction profile intensities for $LiReO_3$. Under the profile for each of the five detectors, plotted on the same scale, are the differences between the observed and calculated profiles.

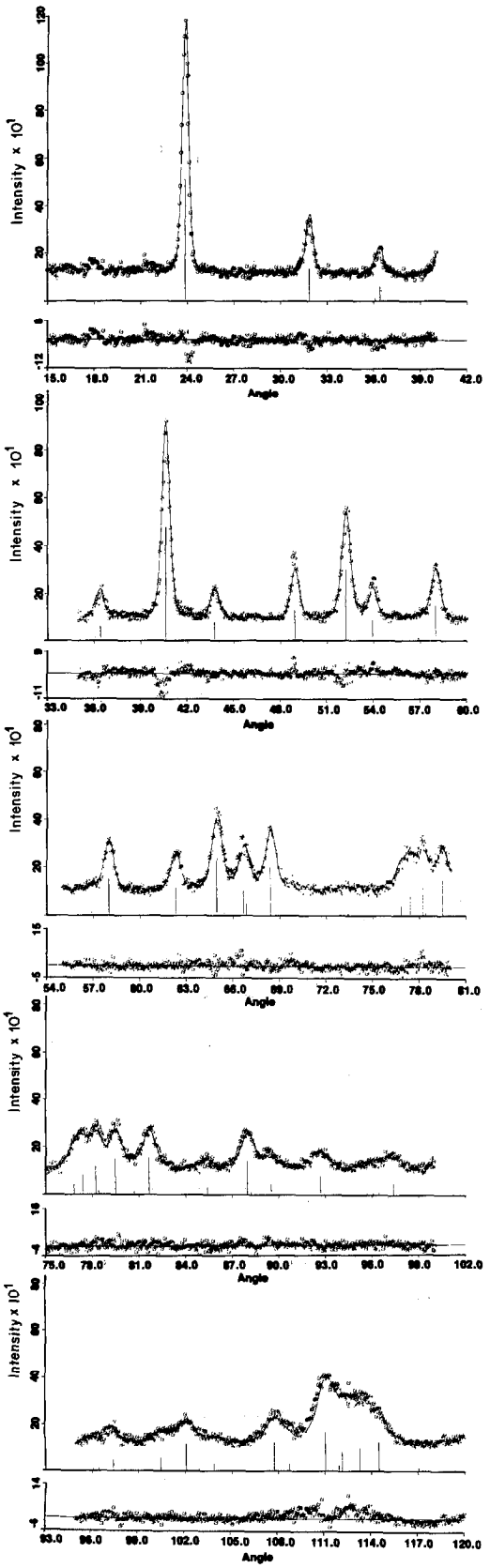

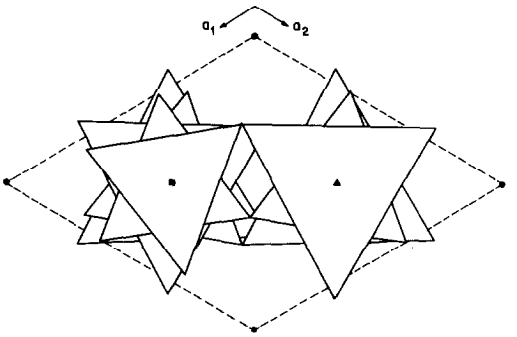

FIG. 3. The structure of $LiReO_3$ projected into the (001) plane. The shared triangular faces of two of the chains of MO_6 octahedra which run parallel to c are emphasized with bold lines. Obscured faces are not shown. Oxygen atoms are at the vertices of the triangles, and the metal atom positions, which project to (0, 0), ($\frac{1}{3}$, $\frac{2}{3}$), and ($\frac{2}{3}$, $\frac{1}{3}$), are occupied along c as follows: ●,▲ = Re–vacancy–Li1–Re–vacancy–Li1; ■ = vacancy–Li1–Re–vacancy–Li1–Re.

model and the data (see Table III and Fig. 2). The lineshapes in this case are close to modified Lorentzians. Again, there are six formula units per hexagonal cell. Both Li and Re were found to occupy positions of the type 6*a* (in this case there are two independent Li atom positions), and oxygen is in the general position 18*b*. Atomic positions and thermal parameters for the Li_2ReO_3 structure are presented in Table III B.

The structure of Li_2ReO_3 is very similar to that of $LiReO_3$, except that all of the face-shared MO_6 octahedra are now occupied. Beginning with the Re at (0, 0, 0), the MO_6 octahedra are occupied in the order Re–Li1–Li2–Re–Li1–Li2 along the c axis. A projection of the structure down c is presented in Fig. 4. The MO_6 octahedra are again irregular, but much less so than in $LiReO_3$. The addition of the Li atoms to the formerly vacant octahedra has expanded

FIG. 2. Observed and calculated powder neutron diffraction profile intensities for Li_2ReO_3. Under the profile for each of the five detectors, plotted on the same scale, are the differences between the observed and calculated profiles.

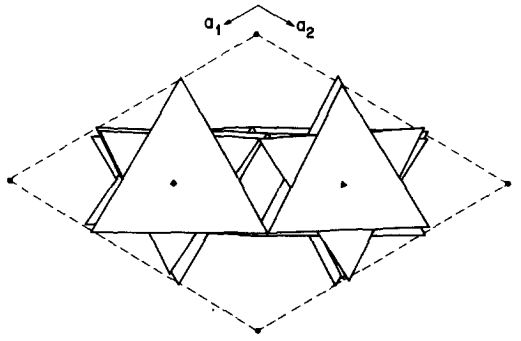

FIG. 4. The structure of Li_2ReO_3 projected into the (001) plane. The shared triangular faces of two of the chains of MO_6 octahedra which run parallel to c are emphasized as in Fig. 3. Oxygen atoms are at the vertices of the triangles, and the metal atom positions are occupied along c as follows: ●,▲ = Re–Li2–Li1–Re–Li2–Li1; ■ = Li2–Li1–Re–Li2–Li1–Re.

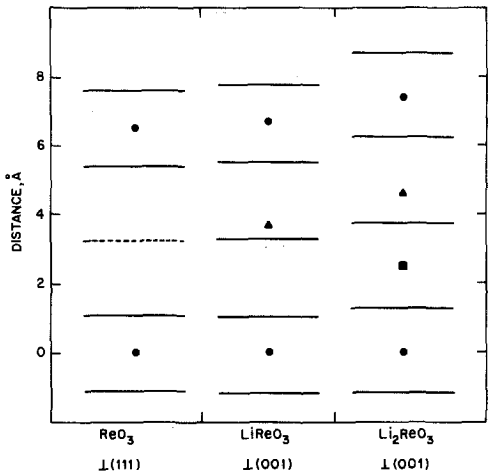

FIG. 5. The structures of ReO_3, $LiReO_3$, and Li_2ReO_3 compared perpendicular to the planes of oxygen atoms. The (111) direction is vertical for ReO_3, and the c axis is vertical for $LiReO_3$ and Li_2ReO_3. Oxygen planes are represented by horizontal lines, and Re, Li1 and Li2 atoms by circles, triangles, and squares, respectively. This figure represents the structures perpendicular to the representations in Figs. 3 and 4.

the structure significantly along c, as illustrated in Fig. 5.

Atomic Coordination

The pertinent bond lengths and angles for the characterization of the rhenium–oxygen and lithium–oxygen coordination polyhedra are presented in Table IV. In both compounds, the ReO_6 octahedra are slightly distorted, as reflected by the small deviations from equality of the two sets of Re–O bond distances and by the deviations by only a few degrees of the bond angles from those of a perfect octahedron. Employing the 1.40-Å ionic radius of oxygen, and the average Re–O separations, we obtain: $R^{VI}_{Re^{4+}} = 0.63(2)$ from Li_2ReO_3, $R^{VI}_{Re^{5+}} = 0.54(1)$ from $LiReO_3$, and $R^{VI}_{Re^{6+}} = 0.48$ from ReO_3. These are in good agreement with the Shannon and Prewett (*15*) radii, except for the radius of Re^{6+}, which we obtain from the lattice parameter of ReO_3. The rhenium coordination in both compounds is more regular than the Nb coordination in $LiNbO_3$, where the Nb is displaced toward one shared face of the octahedron (*14*).

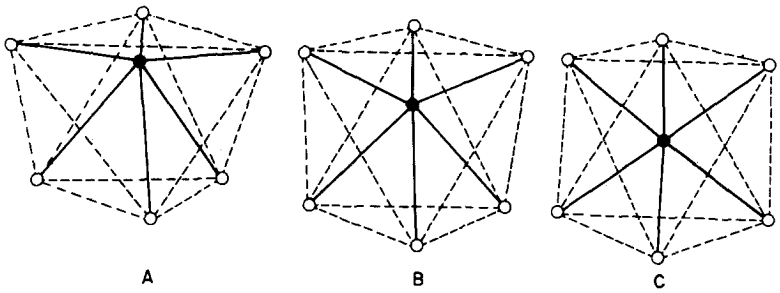

FIG. 6. Lithium coordination polyhedra. Lithium atoms are represented by solid circles, oxygen by open circles. (A) Li in $LiReO_3$, (B) Li1 in Li_2ReO_3, (C) Li2 in Li_2ReO_3. The polyhedra are presented with the c unit cell axis vertical.

The coordination geometries of the lithium atoms are more irregular than those of the rhenium. In $LiReO_3$, the lithium–oxygen bond distances are 2.00(1) and 2.42(1) Å, with some bond angles considerably distorted from those of an octahedron. The coordination is shown in Fig. 6A. The lithium is displaced away from the face it shares with the rhenium–oxygen octahedron, suggesting Re–Li repulsion. In Li_2ReO_3, the lithium–oxygen separation has decreased on the average, with the distances 1.95(1) and 2.30(2) Å for Li1 and 1.98(1) and 2.17(1) Å for Li2. These coordinations are illustrated in Figs. 6B and C, respectively. In Li_2ReO_3 all face-shared octahedra in the chain are occupied, and the more regular Li coordinations suggest that the Li–Li repulsion is comparable to the Li–Re repulsion. Comparison of Li–O distances found in this study to those found in similar materials is not straightforward due to confusion in the literature concerning whether a lithium has actually been located or whether its position has been implied. However, the distances found in $LiNbO_3$, 2.07(1) and 2.04(2) (*14*), are com-

TABLE IV

A. Bond lengths and angles of $LiReO_3$

	Distance	Number
Li coordination polyhedron		
Li–O	2.000(6)	3
	2.42(1)	3
	Angle	
O–Li–O	116.8(3)	3
	85.4(3)	3
	75.3(3)	3
	66.5(5)	3
	139.0(8)	3
Re coordination polyhedron		
	Distance	
Re–O	1.927(8)	3
	1.945(7)	3
	Angle	
O–Re–O	87.0(4)	3
	90.8(1)	
	89.1(1)	3
	93.0(4)	3
	175.6(6)	3
Metal–metal distance		
Li–Re	3.04(2)	

TABLE IV—*Continued*

B. Bond lengths and angles of Li_2ReO_3

	Distance	Number
Li1 coordination polyhedron		
Li1–O	1.95(1)	3
	2.30(2)	3
	Angle	
O–Li1–O	102.8(6)	3
	90.5(3)	3
	87.6(2)	3
	75.9(6)	3
	160.7(9)	3
Li2 coordination polyhedron		
	Distance	
Li2–O	1.98(1)	3
	2.17(1)	3
	Angle	
O–Li2–O	93.9(1)	3
	87.4(6)	3
	89.7(2)	3
	89.1(6)	3
	176.8(3)	3
Re coordination polyhedron		
	Distance	
Re–O	2.01(1)	3
	2.05(1)	3
	Angle	
O–Re–O	90.1(4)	3
	92.4(2)	3
	93.7(1)	3
	83.6(4)	3
	175.5(6)	3
Metal–metal distances		
Li1–Re	2.78(1)	
Li2–Re	2.50(1)	
Li1–Li2	2.11(4)	

parable to those found here. The Li–Re separation in $LiReO_3$ (3.04(2) Å) shrinks considerably in Li_2ReO_3 (2.78(1) and 2.50(1) Å), where there are no vacancies in the cation chain. The Li–Li separation in Li_2ReO_3, 2.11(4) Å, is shorter than that in Li_2O, 2.31 Å.

Discussion

There is a close relationship between the structures of ReO_3, $LiReO_3$, and Li_2ReO_3. The ReO_3 host lattice in the lithium-inserted phases can be derived from that of ReO_3 by a rotation of approximately 60° about a cubic ⟨111⟩ direction, with the shared corners of the ReO_6 octahedra acting as hinges. No bonds are broken. For a rotation of exactly 60°, the transformation is from a ¾ cubic close-packed (CCP) anion array to a hexagonal close-packed (HCP) anion array. Rotations of less than 60° result in an anion-packing intermediate between ¾ CCP and HCP. The resulting phases have rhombohedral symmetry, with the cubic ⟨111⟩ rotation axis becoming the hexagonal c axis. The geometry of the transformation is illustrated in Fig. 7 for the ideal ¾ CCP-to-HCP twist. The geometry of the ⟨111⟩ twist has been discussed by several authors, particularly in reference to the transition metal trifluorides (*16, 17*) and rhombohedral perovskites (*18, 19*). Megaw, in fact, proposed (*20*) that a transition of this sort might be responsible for the ferroelectric transition in $LiNbO_3$, which was later shown to involve a different type of distortion (*21*).

The entire range of structures between ¾ CCP and HCP is observed in the transition metal trifluorides (*16*). Coordinates characterizing the anion array for several of these compounds are presented in Table V, with the coordinates of $LiReO_3$, Li_2ReO_3, and $LiNbO_3$ added for comparison. MoF_3 and TaF_3 have the cubic ReO_3 structure, space group $Pm3m$, with M in (0, 0, 0) and F in (½, 0, 0) (0, ½, 0) (0, 0, ½). These structures can also be described in a hexagonal cell of symmetry $R\bar{3}c$ with cations in (0, 0, 0) (0, 0, ½) and anions in $\pm[(u, 0, \frac{1}{4})$ $(0, u, \frac{1}{4})$ $(\bar{u}, \bar{u}, \frac{1}{4})]$ with $u = -0.5$, which allows comparison to the partially and completely twisted trifluorides. RhF_3 has a perfectly hexagonal close-packed anion array, space group $R\bar{3}c$ with fluorine in the $(u, 0, \frac{1}{4})$-type position with $u = -0.333$.

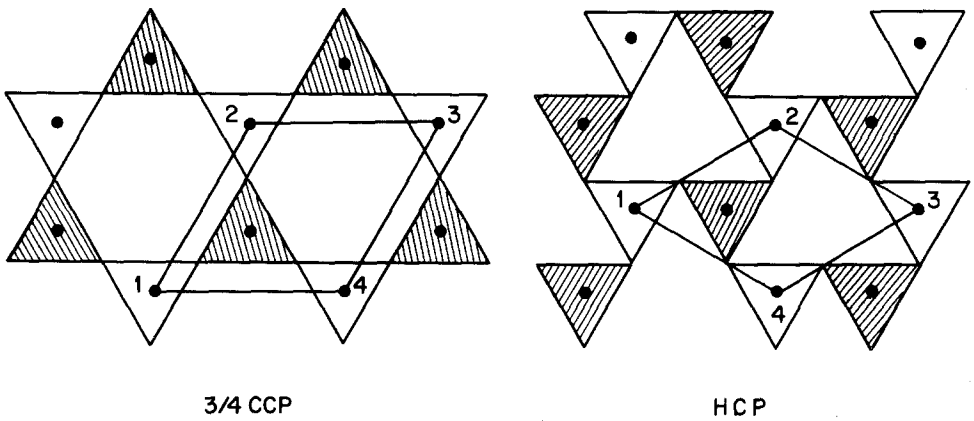

FIG. 7. The transformation by ⟨111⟩ twist between ¾ CCP and HCP, viewed in the cubic (111) and hexagonal (001) planes. Cations for the MX_3-type host lattice are shown as solid circles and the triangles are the triangular faces of the MX_6 octahedra sharing corners (oxygen atoms are at the vertices). Shaded triangles are associated with octahedra above the plane of the figure, and unshaded triangles, octahedra below.

TABLE V

ANION-PACKING COORDINATES IN MF_3-TYPE MATERIALS

Material	Hexagonal cell	Symmetry, packing
MoF_3	−0.500	$Pm3m$, ¾ CCP
ReO_3	−0.500	$Pm3m$, ¾ CCP
TiF_3	−0.433	$R\bar{3}c$, intermediate
CrF_3	−0.386	$R\bar{3}c$, intermediate
$LiReO_3$	−0.380	$R3c$, intermediate
$LiNbO_3$	−0.371	$R3c$, intermediate
Li_2ReO_3	−0.358	$R3c$, intermediate
RhF_3	−0.333	$R\bar{3}c$, HCP

Note. u in $(u, 0, \frac{1}{4})$.

TABLE VI

COMPARISON OF $LiNbO_3$, $LiReO_3$, AND Li_2ReO_3 STRUCTURES

	$LiNbO_3$	$LiReO_3$	Li_2ReO_3
a	5.148	5.092	4.971
c	13.863	13.403	14.788
In (0, 0, x)			
Li	0.280	0.273	0.312
	—	—	0.169
Re, Nb	0.0	0.0	0.0
In (x, y, z)			
Oxygen			
X	−0.3709	−0.3801	−0.358
Y	0.0102	0.012	−0.008
Z	0.2299	0.246	0.2551

For values of u between −0.5 and −0.333, the degree of twist is between ¾ CCP and HCP. For example, Table IV includes distorted CCP TiF_3, $u = -0.433$, and distorted HCP CrF_3, $u = -0.386$. The lithium rhenates and niobates are not centrosymmetric and thus the coordinates $(u, 0, \frac{1}{4})$ in Table IV are approximate. The anion arrays are intermediate in packing, with that of Li_2ReO_3 at $u = -0.358$, close to perfect HCP. The similarity of the $LiNbO_3$, $LiReO_3$, and Li_2ReO_3 structures is further illustrated in Table VI. The positions of the atoms in $LiNbO_3$ have been included[1] (*14*) to facilitate comparison.

For ideal hexagonal close-packing of anions, the anions at different z in the unit cell project to exactly the same location on the (001) plane (see Fig. 7). This does not happen in $LiReO_3$ and Li_2ReO_3, due to distortions of the shapes and rotations of the octahedra (Figs. 3 and 4). A measure of the perfection of the hexagonal packing is in the metal–oxygen–metal bond angle projected into the (001) plane for neighboring corner-shared octahedra. In the cubic case, this angle is 180°, and for the ideal hexagonal close-packed case, it is 120°. In both $LiReO_3$ and Li_2ReO_3 the metal–oxygen–metal angles display a range of values about that corresponding to perfect hexagonal close-packing: 107–143° for $LiReO_3$ and 115–124° for Li_2ReO_3.

The twist in the ReO_3 host lattice occurs to accommodate the coordination preferred by the Li ions, and is possible because of the exclusive corner sharing. The change in shape of the interstitial cavity is illustrated in Fig. 8. In ReO_3 the cavity is a cubo-octahedron, and the center is 12-coordinated. The ⟨111⟩ twist converts the 12-coordinate cavity into two 6-coordinate (octahedral) cavities sharing faces. The volume per formula unit decreases in going from ReO_3 to $Li_{0.35}ReO_3$ (see Table II), stays approximately the same on further lithium insertion and twisting to the rhombohedral cell, and then increases on further Li insertion so that the volume of Li_2ReO_3 is approximately equal to that of ReO_3. These volume changes reflect both the increased packing density of the anion array and the changes in the sizes of the cation coordination polyhedra.

Compounds which have been observed to undergo twists of the type described here are relatively few. In addition to the present examples, compounds of stoichiom-

[1] The reported $LiNbO_3$ coordinates are transformed to the present coordinates by: $X = (Y_{LN} - X_{LN}) + \frac{1}{3}$, $Y = Y_{LN} + \frac{2}{3}$, $Z = Z_{LN} + \frac{1}{6}$.

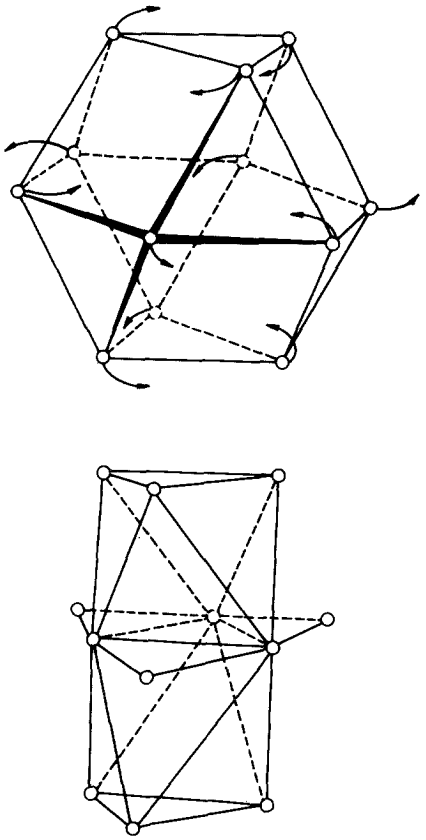

FIG. 8. The twist of the 12-coordinate cavity in ReO_3 to form two octahedra sharing faces, as found in $LiReO_3$ and Li_2ReO_3.

etry $M^{II}M^{IV}F_6$ (ordered ReO_3 type) have been observed to undergo cubic-to-hexagonal transitions (*22*), and $LiNbO_3$ and $LiTaO_3$ (rhombohedral) have been observed to become cubic on ion exchange of hydrogen for lithium (*23*).

Conclusion

We show that on lithium insertion into ReO_3 the ReO_3 host lattice undergoes extensive deformation, through twisting, to form more favorable coordination sites (nearly octahedral) for the inserted lithium. Although this deformation involves no bond breaking, it is a much more significant structural change than has been observed in other insertion compounds in which sites were present but vacant in the host.

The flexibility of the ReO_3 structure arises from the exclusive corner sharing of the $[ReO_6]$ units. Shear structures related to ReO_3 contain both corner- and edge-sharing units, which would be expected to make twisting on lithium insertion more difficult. This is demonstrated in the stability of the host lattice of $Li_2FeV_3O_8$, whose structure we have determined by neutron diffraction powder profile analysis (*9*). The details of that structure will be presented elsewhere.

References

1. M. S. WHITTINGHAM, *Progr. Solid State Chem.* **12**, 1 (1978).
2. J. O. BESENHARD AND R. SCHÖLLHORN, *J. Power Sources* **1**, 267 (1976).
3. D. W. MURPHY AND P. A. CHRISTIAN, *Science* **205**, 651 (1979).
4. D. W. MURPHY, P. A. CHRISTIAN, J. N. CARIDES, AND F. J. DISALVO, *in* "Fast Ion Transport in Solids" (P. Vashishta, J. N. Mundy, and G. K. Shenoy, Eds.), pp. 137–140, North-Holland, New York (1979).
5. D. W. MURPHY, M. GREENBLATT, R. J. CAVA, AND S. M. ZAHURAK, *Solid State Ionics* **5**, 327 (1981).
6. J. R. DAHN, W. R. MCKINNON, R. R. HAERING, W. J. L. BUYERS, AND B. M. POWELL, *Canad. J. Phys.* **58**, 207 (1980).
7. P. J. WISEMAN AND P. G. DICKENS, *J. Solid State Chem.* **17**, 91 (1976).
8. D. COX, R. J. CAVA, D. B. MCWHAN, AND D. W. MURPHY, *J. Phys. Chem. Sol.*, in press.
9. R. J. CAVA, A. SANTORO, D. W. MURPHY, S. M. ZAHURAK, AND R. S. ROTH, *Solid State Ionics* **5**, 323 (1981).
10. H. M. RIETVELD, *J. Appl. Crystallogr.* **2**, 65 (1969).
11. E. PRINCE, "U.D. Tech. Note 1117 (F. J. Shorten, Ed.), pp. 8–9, National Bureau of Standards, Washington, D.C. (1980).
12. A. SANTORO, R. J. CAVA, D. W. MURPHY, AND R. S. ROTH, "Proceedings, Symposium on Neutron Scattering, Aug. 12, 1981, Argonne, Illinois." American Institute of Physics, in press.
13. G. E. BACON, *Acta Crystallogr. Sec. A* **28**, 357 (1972).
14. S. C. ABRAHAMS, J. M. REDDY, AND J. L. BERNSTEIN, *J. Phys. Chem. Solids* **27**, 997 (1966).

15. R. D. SHANNON AND C. T. PREWETT, *Acta Crystallogr. Sect. B* **25,** 925 (1969).
16. M. A. HEPWORTH, K. H. JACK, R. D. PEACOCK, AND G. J. WESTLAND, *Acta Crystallogr.* **10,** 63 (1967).
17. A. F. WELLS, "Structural Inorganic Chemistry," p. 214, Oxford Univ. Press, London/New York (1975).
18. H. D. MEGAW AND C. N. W. DARLINGTON, *Acta Crystallogr. Sect. A* **31,** 161 (1975).
19. M. O'KEEFFE AND B. G. HYDE, *Acta Crystallogr. Sect. B* **33,** 3802 (1977).
20. H. D. MEGAW, *Acta Crystallogr.* **7,** 187 (1954).
21. S. C. ABRAHAMS, H. J. LEVENSTEIN, AND J. M. REDDY, *J. Phys. Chem. Solids* **27,** 1019 (1966).
22. J. PEBLER, D. REINEN, K. SCHMIDT, AND F. STEFFENS, *J. Solid State Chem.* **25,** 107 (1978).
23. C. E. RICE AND J. L. JACKEL, *J. Solid State Chem.* **41,** 308–314 (1982).